AIAA JOURNAL
Vol. 45, No. 10, October 2007

Surrogate-Based Aerodynamic Shape Optimization of a Civil Aircraft Engine Nacelle

Wenbin Song* and Andy J. Keane†
University of Southampton, Southampton, SO17 1BJ England, United Kingdom

DOI: 10.2514/1.30015

In this paper, we present a study on the aerodynamic shape optimization of a three-dimensional subsonic engine nacelle using computational fluid dynamics simulations. Gaussian process-based surrogate modeling (kriging) and parameter screening techniques are combined to tackle the high cost associated with both computational fluid dynamics simulations and the large number of design variables involved, with a multi-objective genetic algorithm being used to obtain the Pareto fronts. The primary goal of the study was to identify the tradeoff between aerodynamic performance and noise effects associated with various geometric features within practical computational costs. The fan face total pressure recovery is used to measure the aerodynamic performance, and the scarf angle is used as an indicator of the noise impact on the ground. The geometry is modeled using a feature-based parametric computer-aided design package. An unstructured tetrahedral mesh is generated for the subsequent solution using the Reynolds averaged Navier–Stokes flow equations. Analyses of variance techniques are used to identify the dominant geometry parameters, thereby reducing the number of design variables and computational cost in the trade study. Multiple Pareto fronts are constructed using progressively built kriging models based on simulation data with the reduced parameter set. A full-scale search was also carried out for comparison with the results produced using the reduced parameter set. The procedures outlined can be further applied to other optimization problems with significant numbers of parameters and high-fidelity analysis codes.

Nomenclature

m	=	number of data points
n	=	number of dimensions
p_k	=	kriging hyperparameters
R	=	correlation function
$\mathbf{x}$	=	design variable vector
y	=	function value
Z	=	zero mean stationary Gaussian random function
β	=	constant
θ_k	=	kriging hyperparameters
μ	=	main effect of variables
σ^2	=	variance

Subscript

k	=	index of dimensions

Superscripts

i	=	index of design point
j	=	index of design point

I. Introduction

CONSTRAINTS on aircraft noise are becoming increasingly important in the design of commercial aircraft and engines. To meet the current and future Federal Aviation Regulations (FARs) on noise footprint, while at the same time providing sufficient power to meet the demand of new larger aircraft, methods are needed to reduce noise levels while maintaining aerodynamic performance and satisfying installation and power requirements. A recent survey on various noise reduction technologies can be found in Fisher and Self [1]. Aspects such as active noise control, passive or adaptive acoustic liners [2], and geometry redesign of the engine nacelle are all being studied. The feature considered here is the introduction of a negative scarf angle at the engine inlet plane, thus transforming the nacelle from only moderately three dimensional to strongly three dimensional in terms of inlet length [3–6]. The geometries of a typical positive scarfed nacelle (+5 deg) and a negative scarfed nacelle (−10 deg) are illustrated in Fig. 1. The full descriptions of the variables in the figure are given in Table 1.

The inlet geometry of the jet engine governs the airflow into the fan and thus plays a significant role in fan noise radiation as well as engine performance. It is therefore important to understand the design implications of a negative scarf angle at low and transonic speeds. A staged and iterative method for studying this problem was described by Nangia and Palmer [4]. This led to a negatively scarfed lip with the same attached flow capacity as a conventional inlet for low and subsonic speed operations. A second paper by Nangia and Palmer focused on the lip shaping in the transonic speed range [5]. Optimization was identified in the paper as the logical next step for the design of nacelles with negative scarf angles. A computational study of the aerodynamic performance of three-dimensional subsonic inlets was performed by Abbott and Slater [3] with attention focused on three design parameters including the inlet internal lip thickness, the axial extent of the lower lip extension, and the circumferential extent of the transition from the extended lower lip to the nonextended upper lip. The latter two parameters characterize the feature of a negative scarf angle, which has drawn much attention in the acoustic noise reduction community. The design problem has also been studied using optimization techniques and computational fluid dynamics (CFD) codes; for example, a subsonic inlet shape optimization was performed by Mason et al. [7] using an orthogonal array approach and polynomial response surface models for various operating conditions. The same configuration was studied by Reddy [6] using a modified quasi-Newton gradient-based method (BFGS: Broydon–Fletcher–Goldfarb–Shanno) to minimize the peak Mach number on the inside of the inlet surface with the lip profile parameters chosen as design variables. However, the number of variables used in these studies tends to be relatively small and were primarily focused on local shape change. In addition to

Received 25 January 2007; accepted for publication 16 June 2007.

*Research Fellow, School of Engineering Sciences. Member AIAA.
†Professor of Computational Engineering, School of Engineering Sciences.

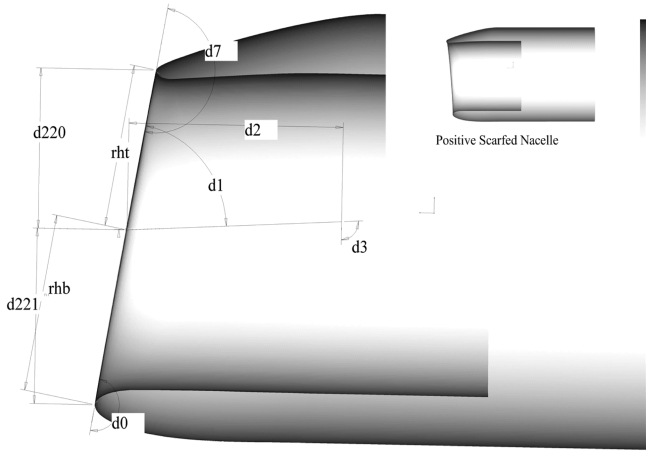

Fig. 1 Geometries of negatively and positively scarfed nacelles.

computational studies, some experimental work was also reported under the European Framework 6 Programme SILENCE [8].

It is important to understand both the benefits of a negative scarf angle in noise reduction and its downside on aerodynamic characteristics. The advantages of introducing a negative scarf angle lie mainly in an increased angle of attack capability in terms of pressure distortion at the fan face and a reduction in ground vortex strength, whereas the disadvantage is mainly shown by the limited attached flow ranges under crosswind conditions. When studying the aerodynamic effects of negative scarf, several different aspects can be chosen to measure the performance of the nacelle, including pressure distribution at the engine face. However, these performance measures are not only affected by geometry changes; for example, pressure distortion at the fan face can also be caused by an internal lip flow separation, a shock-induced flow separation at the throat, or a flow separation from the diffuser wall. Therefore, performance needs to also be assessed in terms of attached flow ranges using the onset of lip flow separation predictions. This leads to a multicriteria optimization study for the problem. However, in this paper, the focus is on the single most important aerodynamic performance characteristic, that is, the total pressure recovery at the fan face.

An iterative design method was presented by Nangia and Palmer [4] to accommodate subsonic, transonic, supersonic, incidence, and side-slip conditions arising from typical transport engine operating envelopes. The importance of each condition is considered by the place of the individual loop in the design process. Low speed (takeoff, landing) was considered most important, and thus lies in the innermost loop which is iterated until environmental constraints are satisfied before going to the next loop. Side-slip effects at low speed are the next most important, for which certification requirements have to be met. The next factor is the economic considerations at a cruise condition where low drag and high inlet efficiency become the driving factors. Although this iterative process will lead to an improvement in the design, it offers little insight into the effect of

Table 1 Design variables for engine nacelle geometry

Index	Name	x_l[a]	x[b]	x_u[c]	Description
1	Scarf angle*	−25	5	10	Negative scarf angle, deg
2	Teaxis	5	12	20	Axial coordinate of top external profile, mm
3	Telater	5	10	20	Radial coordinate of top external profile, mm
4	Beaxia	10	18.5	20	Axial coordinate of bottom external profile, mm
5	Belater	10	19	20	Radial coordinate of bottom external profile, mm
6	Seaxis	5	10	15	Axial coordinate of side external profile, mm
7	Selater	10	15	20	Radial coordinate of side external profile, mm
8	Tiaxis	1.5	2	2.5	Ratio of top inner profile coordinate
9	Tilater*	1	1.34	1.6	Coefficient of top inner profile coordinate in lateral direction
10	Biaxis	2.5	2.8	3.0	Ratio of bottom inner profile coordinate
11	Bilater*	1.0	1.27	1.5	Coefficient of bottom inner profile coordinate in lateral direction
12	Siaxis	2	2.45	3	Ratio of side inner profile coordinate
13	Silater*	1	1.34	1.6	Side inner profile coordinate in lateral direction, mm
14	Droop	−5	0	5	Droop angle of axial axis, deg
15	d220*	1100	1243	1300	Top lip radius, mm
16	d221*	1300	1360	1400	Bottom lip radius, mm
17	rhs*	1400	1430	1500	Side lip radius, mm
18	d122	1700	1750	1800	Bottom lip axial length, mm
19	d119	1800	1850	1900	Top lip axial length, mm
20	d115	1800	1825	1900	Axial length of highlight plane center, mm
21	rmt	1700	1710	1800	Top lip endpoint radius, mm
22	rmb	1600	1625	1700	Bottom lip endpoint radius, mm
23	d124	3300	3340	3400	Nozzle axial length, mm
24	d138	85	90	95	Nozzle exit angle, mm
25	d126	−5	0	5	Nozzle endpoint offset, mm
26	d90	40	50	60	Forward length of inner barrel, mm
27	d92	600	620	650	Half-length of inner barrel, mm
28	d225	22	25.4	28	Radial control length of top lip profile, mm
29	d226	22	25.4	28	Axial control length of top lip profile, mm
30	d235	22	25.4	28	Radial control length of bottom lip profile, mm
31	d236	22	25.4	28	Axial control length of bottom lip profile, mm
32	d230	22	25.4	28	Radial control length of side lip profile, mm
33	d231	22	25.4	28	Axial control length of side lip profile, mm
34	d0	——	180	——	Control parameter, deg
35	d1	——	85	——	90-scarf angle, deg, dependent variable
36	d2	——	1775	——	Reference axial dimension, mm
37	d3	——	95	——	Control parameter, deg
38	d7	——	180	——	Control parameter, deg
39	rht	——	1262	——	Dimension of the top half inlet, mm
40	rhb	——	1360	——	Dimension of the bottom half inlet, mm

[a]Lower bounds of design variables.
[b]Base values of design variables.
[c]Upper bounds of design variables.

many of the geometry parameters on the design, and the overall design space shape is still very much unknown. Another problem with the above approach is that the time-consuming inner loops may be visited more than once, and only a few discrete design points can be considered for running a computational fluid analysis.

An inverse design procedure was presented by Wilhelm [9], in which an iterative residual-correction-type approach was adopted to modify the geometry to produce a required pressure distribution. The calculated geometry difference needed to be smoothed and added to the original geometry in terms of node coordinates; therefore, careful mesh manipulation was necessary to generate computational meshes for the modified nacelle geometry. Large geometry changes cannot be accommodated in this type of process as they may bring significant challenges to the mesh manipulation algorithms. In addition, this method lacks the ability to smooth the original geometry: pressure fluctuations caused by nonsmooth curvature distributions will cause difficulties in achieving the target pressure distribution while the average pressure distribution may be matched quite well. Ideally, a parametric CAD geometry needs to be incorporated in the process to drive the design modification process.

CFD codes coupled to a parametric CAD geometry and numerical optimization methods can be used in the design process to systematically improve designs. However, there are still many challenges to overcome to achieve an efficient and robust design process due to reasons such as the lack of robust design automation and the high computational cost associated with large numbers of iterations of high-fidelity CFD analysis. Robust and automatic mesh generation remains as one of the major bottlenecks in applying optimization techniques to aerodynamic shape design using CAD and CFD.

The use of response surface modeling and multi-objective genetic algorithms, supported by high performance computing facilities, has drawn increasing attention in the design community to tackle the CFD-based shape optimization problems. For example, Lian and Liou [10] used polynomial response surface methods and evolutionary multi-objective algorithms for turbopump blade optimization. However, the number of design variables in many applications of these approaches are relatively small, typically below 20.

The aim of this paper is to present a generic design approach for the study of various geometric parameters on a subsonic engine nacelle, especially the effect of a negative scarf angle. The system is implemented within the MATLAB©[‡] scripting environment leveraging three key components: response surface modeling, parameter screening, and a multi-objective genetic algorithm. The paper is organized as follows: the next section presents a brief overview of past work in related fields. Section III describes the optimization problem, parameter screening using surrogate models and optimization studies. Section IVfour describes the optimization study using a subset of the geometry parameters identified in the screening process of Sec. III. Conclusions are presented in the final section.

II. Past Work

Although a negative scarf angle is of interest primarily to tackle complex noise reduction problems, the formulation in the current paper is based on a simple assumption that the larger the scarf angle, the lower the noise level below the engine. Therefore, the focus in the current work is to maximize both the total pressure recovery at the fan face and the scarf angle at the same time. The computational cost involved in such studies is a function of the flow model and mesh size. For example, Navier–Stokes solvers require more computational time than Euler solvers, but provide more accurate results. It is, of course, always desirable to use the most accurate models, but constraints on design cycle time and computing resources mean that less accurate low-fidelity models are often used. In such cases, experimental data or high-fidelity models can be used to calibrate the low-fidelity model. Even so, a simplification of the analysis models may not produce satisfactory results despite the help of statistical design of experiment methods, as shown in [6].

A. Response Surface Methods

The high computational cost of high-fidelity analysis codes has prompted numerous research efforts using response surface models for various optimization problems. There exist a number of methods for building such metamodels. Jin [11] provided a comprehensive survey on the various methods for use with evolutionary computation methods, among which the radial basis function (RBF) and kriging (Gaussian-based approach) attracted the most attention due to their effectiveness in dealing with results from computational simulations. The kriging method is statistically more meaningful and allows the possibility of computing error estimates for untried data points; therefore, the method has seen wide use in aerospace applications. However, one of the drawbacks of the kriging approach is the relatively high computational cost in estimating the hyperparameters of the model, especially when a large number of sample points are used.

B. Multi-Objective Optimization

The vast majority of real-world design problems can be better solved using multi-objective tradeoffs and optimizations as these complex problems typically have conflicting targets, such as performance, cost, and environmental impact. Evolutionary computation methods have proved to be both effective and efficient in dealing with multiple objectives compared to traditional approaches using single aggregated objective measures based on weighting metrics. Because of their effectiveness, the methods have been applied in a variety of applications including structural [12] and flow optimization problems [13]. A number of evolutionary-based methods have been proposed in the literature. These techniques include, among others, Pareto envelope-based selection (PESA) [14], Pareto archive evolutionary strategy (PAES) [15], non-dominated sorting genetic algorithm II (NSGA-II) [16], and niched Pareto genetic algorithms (NPGA) [17].

More sophisticated algorithms have also been developed to improve the efficiency of the baseline algorithm, for example, combining the evolutionary search with a local improvement procedure to form hybrid procedures such as M-PAES [18]. An overview on issues, methods, and prospects of the application of memetic algorithms in multi-objective optimization problems was provided by the same authors [19].

C. Geometry Parameterization

High-fidelity multidisciplinary analysis codes often require the modeling of complex geometry with many details, and consistency across all disciplines such as structural analysis and computational fluid dynamics analysis. Robust regeneration of a parametric geometry model lies at the heart of multidisciplinary optimization problems. Such shape parameterization methods in the context of high-fidelity multidisciplinary design optimization have been investigated by a number of researchers. A comprehensive overview on geometry parameterization and its applications was given by Samareh [20]. A combined shape, topology, and configuration optimization for structures was recently reported by Langer et al. [21], in which a parametric model was constructed using the CAD tool Pro/ENGINEER©.[§] In most cases, the transfer of geometry between application codes is by using standard neutral formats such as STEP, IGES, PATRAN, etc. Additional nongeometrical information can also be transferred using the mechanisms available in these standards, and this can be particularly helpful when dealing with topology changes. For example, every geometrical entity was tagged using a unique label in previous work by the authors [22], and later referenced by various analysis tools. However, this method of unique tagging depends on the capability of the various interpreters

[‡]Data available online at http://www.mathworks.com [retrieved 1 May 2007].

[§]Data available online at http://www.ptc.com [retrieved 1 May 2007].

provided by computer-aided engineering (CAE) software vendors, and therefore it is not always available. Moreover, when a top–down design approach is adopted, it may become difficult to reference lower level entities in an imported geometry, which may be required when, for example, specifying edge node spacing during meshing phases. A unified approach for CAD-based geometry handling in support of single and multidisciplinary analysis and design was presented by Haimes and Merchant [23]. The method provides a tightly coupled scenario by eliminating the use of intermediate formats for transferring geometries between CAE packages. Direct access to geometric entities from within CAD using an application programming interface (API) has the potential to support robust and efficient mesh generation for CAE packages. However, further effort is still required for such interfaces to become widely adopted.

Here, a parametric engine nacelle geometry has been defined using Pro/ENGINEER. Around 40 parameters are used in the definition of this model to provide a generic definition, and this enables the study of various geometric features. As already noted, the negative scarf angle is the main focus of this study. Radial dimensions are specified at three circumferential locations: the windward (bottom) plane ($\theta = 0$ deg), side plane ($\theta = 90$ deg), and leeward (top) plane ($\theta = 180$ deg). Parameters considered are focused on those affecting lip inner profiles at three circumferential locations defined at the above locations, where at each point, the inner and external profiles are defined by two parameters resulting in a 33 parameter optimization problem. The parameters used in the geometry definition are listed in Table 1, along with initial values for the parameters. Some of the parameters are also shown in Fig. 1. The asterisks after some of the parameter names label the parameters identified by the parameter screening process described in the current paper as more important than the others.

D. Mesh Generation and CFD Solution

In an automated shape optimization process meshes need to be generated in a closed loop in batch mode based on geometries exported from the parameteric model. Two different approaches can be adopted in an iterative search process involving modified geometries. The first approach involves creating a new mesh from scratch every time the geometry is modified; the second uses mesh manipulation techniques to obtain a new mesh for the modified geometry based on a precreated base mesh on the base geometry. Although the second approach is preferable in terms of its improved numerical efficiency, it is often difficult to accommodate large changes in geometry in the process and it is even more challenging to deal with topology changes. However, this does not imply that the first approach presents no challenge, as it often involves rebuilding detailed topology information in meshing tools using data passed in from CAD or retrieving this information directly from CAD. Both choices are tedious, time consuming, and often applicable only to a specific geometry parameterization.

The first approach is used here to accommodate large changes in geometry in the optimization process. However, when geometries created in CAD are passed into meshing tools using IGES or STEP formats, some "geometry repair" work is almost inevitable to clean up the geometry to create robust, high quality meshes. These operations include removal of undesirable features like very short edges and very small surfaces (via surface or edge merging), and this process is normally interactive in nature involving graphic picking. The use of unique tag names for geometric entities can be seen as an alternative to graphic picking and can also be used to deal with topology changes [24]. However, this is not always possible, especially for complex models generated using a top–down design approach, in which only the top-level geometry entities can typically be directly labeled by the user and subsequently referenced by meshing tools. The underlying entities are usually named automatically by the system in a manner that users typically have no direct control over. In this work, to avoid further geometry manipulations in the meshing tool on the imported geometries, the parametric CAD geometry has been enhanced to prepare it for analysis. Features have been added to extend the inlet exterior surface to the far field at its maximum exterior radius. The regenerated geometry for each set of design variables is transferred into the meshing tool via the use of a STEP file. Meshes are generated in the order of edges, surfaces, and volumes, with mesh controls applied to edges, surfaces, and volumes, respectively, using various edge node spacing schemes and size functions available from the meshing tool GAMBIT© (the FLUENT©[¶] meshing tool). The limitation of this approach is that the top-level topology must remain the same. Also when a different version of the meshing tool is to be used, the script file will often need some modifications due to the different naming of various entities.

Table 2 Mesh sensitivity study results

Index	No. of cells	$\alpha 0$[a]	$\alpha 2$[b]	Time (8 processor · h)	TPR
1	113,458	2.0	1.45	40 min (2 processors)	0.9141
2	300,941	3.5	1.35	1	0.9270
3	469,358	5	1.65	6.5	0.9293
4	505,023	5	1.55	8	0.9303
5	539,251	5	1.45	2	0.9316
6	579,382	5	1.35	2	0.9317
7	1,422,781	8	1.35	9	0.9447
8	2,174,353	10	1.35	10	0.9463

[a]No. of nodes on the shortest edge.
[b]Growth rate of element size.

The intake geometry under consideration here is symmetric about the zero yaw angle. Hence, the mesh generated contains only one-half of the model. The model is then placed into a free flow far-field box. Node spacing is specified on the edges to control the mesh density of the surface and flowfield. A triangular mesh is first generated on the surfaces and a tetrahedral mesh is then generated for the flowfield. To obtain the most appropriate balance between accuracy of the CFD solution and the solution time required for convergence, a mesh sensitivity study is first carried out by varying two main mesh control parameters. The first control parameter ($\alpha 0$) is the number of nodes on the shortest edge; the second control parameter ($\alpha 2$) controls the growth rate of the element size relating to the relative length of the edges against the shortest one. Based on the results shown in Table 2, the control parameter set of (8, 1.35) is chosen for the CFD solutions throughout the remainder of this study. In the current work, FLUENT is used to model the flow around the nacelle. A structured boundary mesh of 18 layers is attached to the surfaces, with the thickness of the first cell set to 0.02 (approximately 0.08% of reference dimension of the nacelle). A flow speed Mach number of 0.85 was used in the simulation. A laminar flow model is solved using a segregated solver from FLUENT.

E. Problem Solving Environment

The design of increasingly complex engineering systems requires increasingly efficient and effective computational environments as well as more computing power. Emerging grid computing techniques seem to be able to provide a general approach for integration and collaboration while retaining the division and autonomy of disciplinary domain experts. To address the organizational challenges that prevent the wide application of a multidisciplinary optimization approach in a generic manner, a flexible environment supporting a powerful scripting language, rich visualization tools, and common mathematical computation capabilities is desirable. In this work, MATLAB is chosen as the scripting environment for the implementation of Grid computing technologies, as a broad spectrum of functions and algorithms for a wide range of functionalities including graphics and graphic user interface (GUI) building features can be found in MATLAB.

A detailed technical discussion on how the system is implemented is beyond the scope of this paper. Technical details can be found in [24]. Different components are linked together by leveraging various Grid technologies. The computational jobs are submitted and managed through the use of an interface to the grid middleware

[¶]Data available on at http://www.fluent.com [retrieved 1 May 2007].

Globus Toolkit 2.4,** implemented as a set of MATLAB functions using the Java CoG.†† A MATLAB interface to the optimization package OPTIONS‡‡ has been developed based on the Java Native Interface§§ to obtain solutions for both constrained and unconstrained problems in the MATLAB environment. The combination of parametric CAD and a Navier–Stokes solver offers the ability to obtain high-fidelity results, while the adoption of Grid technologies can not only simplify the integration of proprietary legacy codes, but can also harness distributed computing power in a consistent and flexible manner.

III. Surrogate-Based Parameter Screening and Optimization

A. Parallel Tuning of Kriging Hyperparameters

The kriging model was identified by Jin [11] to be able to produce better results than other methods under multiple modeling criteria. The choice of the kriging technique in this work is due to the fact that this method not only provides an estimate of the function values, but also an estimate of posterior variance, which can be used to control the frequency and choice of updates. A brief description of the kriging model is provided below and detailed discussions can also be found in the book by Santner et al. [25]. The kriging model is typically expressed as

$$y(\mathbf{x}) = \beta + Z(\mathbf{x}) \tag{1}$$

where β represents a constant term in the model, and $Z(\mathbf{x})$ is a Gaussian random process with zero mean and variance of σ^2. The covariance matrix of $Z(\mathbf{x})$ is given by

$$\operatorname{cov}\left(Z(\mathbf{x}^i), Z(\mathbf{x}^j)\right) = \sigma^2 R(\mathbf{x}^i, \mathbf{x}^j) \tag{2}$$

where σ^2 is the variance of the stochastic process and $R(.,.)$ is a correlation function between two points $\mathbf{x}^i$ and $\mathbf{x}^j$. Different types of correlation functions can be employed as noted by Jones et al. in [2] A commonly used type of correlation function can be expressed as

$$R(\mathbf{x}^i, \mathbf{x}^j) = \prod_{k=1}^{n} \exp\left(-\theta_k |x_k^i - x_k^j|_k^p\right) \tag{3}$$

where n defines the number of design variables, $\theta_k > 0$ and $1 < p_k \leq 2$ are the hyperparameters. Note that the above equation asserts that there is a complete correlation of a point with itself and this correlation decreases rapidly as the two points move away from each other in the parameter space. The choice of $p_k = 2$ would provide enough flexibility for modeling smooth but highly nonlinear functions for most cases, and $p_k = 1$ allows for gradient discontinuities. The hyperparameters θ_k are estimated by maximizing the log-likelihood function given by

$$-\frac{1}{2}\left[n \ln \sigma^2 + \ln |\mathbf{R}| + \frac{1}{\sigma^2}(\mathbf{y}-\mathbf{1}\beta)^T \mathbf{R}^{-1}(\mathbf{y}-\mathbf{1}\beta)\right] \tag{4}$$

where σ^2 and β can be derived using the following equations once the θ_k are given:

$$\hat{\beta} = (\mathbf{1}^T \mathbf{R}^{-1} \mathbf{1})^{-1} \mathbf{1}^T \mathbf{R}^{-1} \mathbf{y} \tag{5}$$

$$\hat{\sigma}^2 = \frac{1}{n}(\mathbf{y} - \mathbf{1}\beta)^T \mathbf{R}^{-1}(\mathbf{y} - \mathbf{1}\beta) \tag{6}$$

A numerical optimization procedure is required to obtain the maximum likelihood estimates (MLE) of the hyperparameters. Once the hyperparameters are obtained from the training data, the function value at a new point can be predicted by

$$\hat{y}(\mathbf{x}^*) = \hat{\beta} + \mathbf{r}^T \mathbf{R}^{-1}(\mathbf{y} - \mathbf{1}\hat{\beta}) \tag{7}$$

along with the posterior variance $s^2(\mathbf{x}^*)$ given by

$$s^2(\mathbf{x}^*) = \sigma^2\left[1 - \mathbf{r}\mathbf{R}^{-1}\mathbf{r} + \frac{(1 - \mathbf{1}^T\mathbf{R}^{-1}\mathbf{r})^2}{(\mathbf{1}^T\mathbf{R}^{-1}\mathbf{1})}\right] \tag{8}$$

where $\mathbf{r}(\mathbf{x}) = R(\mathbf{x}, \mathbf{x}^1), \ldots, R(\mathbf{x}, \mathbf{x}^n)$ is the correlation vector between the new point $\mathbf{x}$ and the training data set.

In the process of building a global kriging model, the tuning of the hyperparameters used in computing the correlation structure in the kriging model can be the most computational expensive part. This will become more difficult, if not impractical, when the response function contains a large number of peaks and valleys for which there is almost no alternative to sampling a large number of data points. However, it is argued that this tends to not happen very often for many real-world engineering design problems. It is also known that the maximum likelihood estimate of the kriging model is highly nonlinear and multimodel. Therefore, appropriate methods need to be used to find optimized hyperparameters which give good agreement in the prediction of function values over the whole design space. Here, a parallel approach making use of a multistart gradient descent search method is used to tune the hyperparameters. The starting values for the gradient search have been generated using a random Latin hypercube sampling [26]. The best point returned by all the gradient search methods is used in the prediction. This will produce reasonably good estimates of the hyperparameters within a time scale which may otherwise only produce a locally optimal set. Figure 2 illustrates the ability of the kriging model to predict function values at new data points, in which the best set of a hyperparameter set from the parallel tuning process is used.

B. Parameter Screening Using Surrogate Models

For problems with a large number of design variables, it is often necessary and always computationally beneficial to reduce the number of design variables being modeled by fixing variables whose effect on the objective functions is small compared to that of others. However, it is not practical to carry out parameter screening using traditional techniques in cases where a high-fidelity simulation code is used. Surrogate models provide a solution to such studies only when the models are sufficiently accurate for estimation, which itself is a challenging task for high dimensional problems. Nevertheless, this approach can provide useful insight into the influences of different variables, and several iterations of the procedure should be able to provide good estimates on the importance of the variables. The use of surrogate models for parameter screening has been investigated by a number of researchers in the past [27–31]. Having obtained a snapshot data set using design of experiment methods, a number of studies can be used to compare the relative importance of the variables. Given m design points $\mathbf{x}_j \in R^N$, $j = 1, \ldots, m$, scaled with lower and upper bounds into the range [0, 1], set

$$\tilde{\mathbf{x}}_j = \mathbf{x}_j - \mathbf{x}_m, \qquad j = 1, \ldots, m \tag{9}$$

where

$$\mathbf{x}_m = \frac{1}{m}\sum_{j=1}^{m} \mathbf{x}_j$$

The parameter impact factor is found by first computing the accumulated objective function values at different levels for each variable, and then taking the squared sum of the vector for each variable. The evolution of parameter impact factors with regard to the number of design points used is shown in Fig. 3, in which the four most important parameters are identified as the scarf angle, tilater, bilater and silater. It is worth noting that this graph can also be used to indicate whether additional data points are required to fully reflect the influence of each variable.

**Data available online at http://www.globus.org/toolkit/downloads/2.4.3/ [cited April 2007].

††Data available online at http://www.globus.org/cog/java/ [cited April 2007].

‡‡Data available online at http://www.soton.ac.uk/~ajk [cited April 2007].

§§Data available online at http://java.sun.com/j2se/1.4.2/docs/guide/jni/ [cited April 2007].

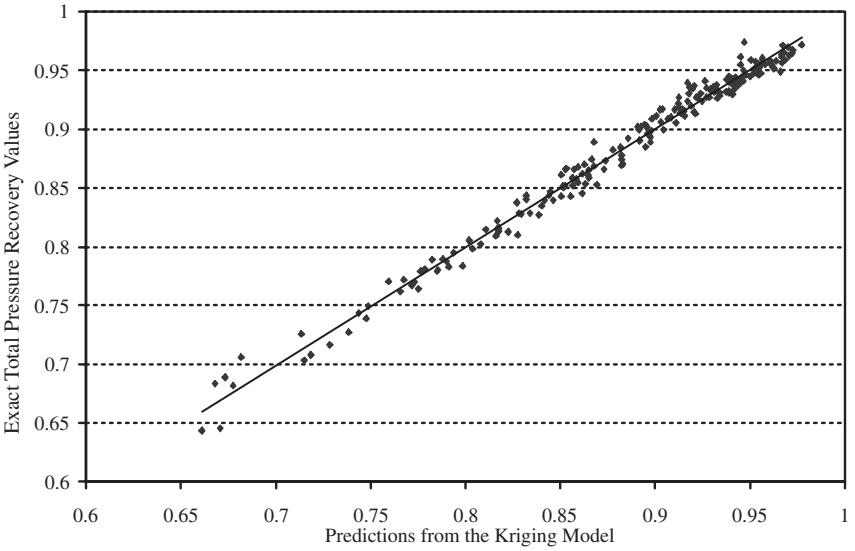

Fig. 2 Correlation between exact function values and predictions from the kriging model on new points.

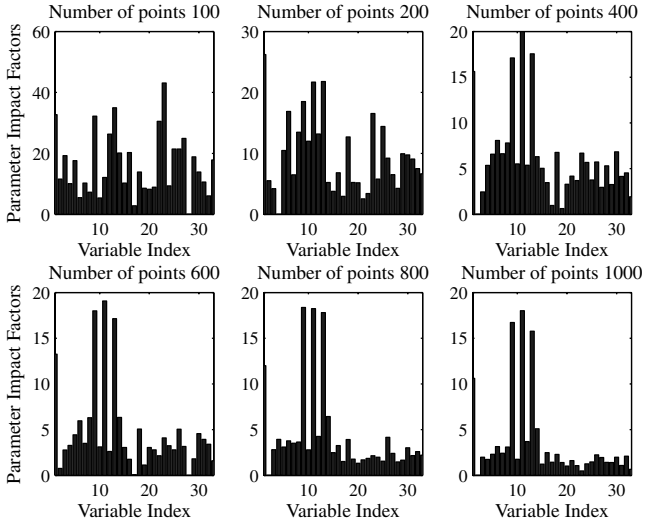

Fig. 3 Estimated impact factor of geometry parameters using the design of experimental data.

The second study uses analysis of variance (ANOVA) techniques [32] on surrogate models to compute the main effect of each design variable. If the surrogate model is represented by $\hat{y}$, the main effect of variable x_i is

$$\hat{\mu}_i(x_i) = \int \cdots \int \hat{y}(x_1, \ldots, x_n)\, \mathrm{d}x_1 \cdots \mathrm{d}x_{i-1} \mathrm{d}x_{i+1} \cdots \mathrm{d}x_n - \hat{\mu} \tag{10}$$

where $\hat{\mu}$ is the total mean of the model, computed as follows:

$$\hat{\mu} = \int \cdots \int \hat{y}(x_1, \ldots, x_n)\, \mathrm{d}x_1 \cdots \mathrm{d}x_n \tag{11}$$

The variance due to the design variable x_i is

$$\int [\hat{\mu}_i(x_i)]^2\, \mathrm{d}x_i \tag{12}$$

The main effect of each variable is computed from the surrogate model built using the best set of hyperparameters and the results shown in Fig. 4. The seven most important variables obtained are identified by an asterisk in Tables 1 and 3 listing all the design variables.

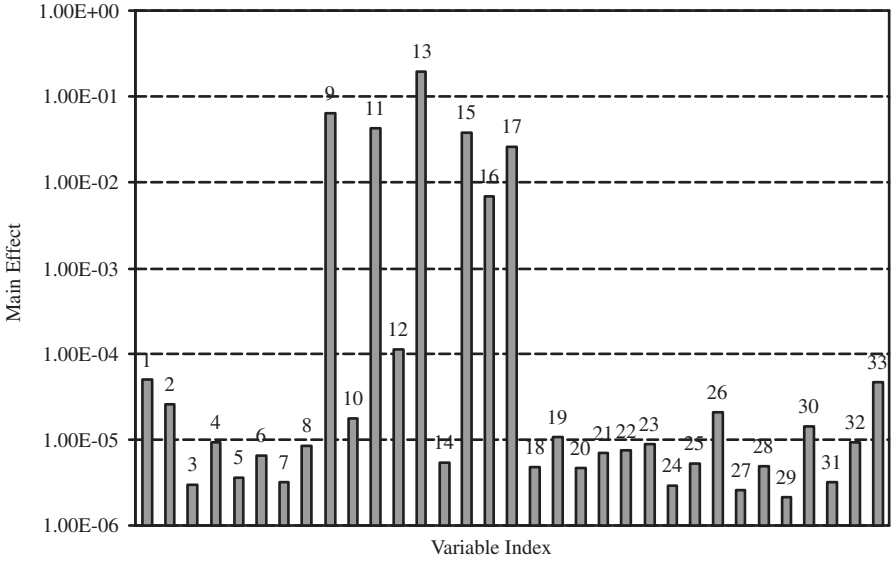

Fig. 4 Main effect analysis of design variables using ANOVA techniques and the kriging model.

Table 3 List of optimal values for all design variables of nacelle geometry

Index	Variables	A[a]	B[b]	C[c]	D[c]	E[c]	F[d]
1	Scarf angle*	3.16	−25	−20.57	−24.94	−25.00	−25.00
2	Teaxis	7.25	16.73	12.98	13.04	10.02	10.02
3	Telater	4.24	5.94	13.33	13.33	13.65	13.65
4	Beaxia	19.53	17.93	16.72	16.72	17.22	17.22
5	Belater	14.92	11.19	17.71	18.96	13.95	13.95
6	Seaxis	6.39	6.11	6.12	6.12	9.88	9.88
7	Selater	14.02	17.11	11.04	11.04	10.06	10.06
8	Tiaxis	1.91	1.56	2.33	2.39	2.31	2.31
9	Tilater*	1.13	1.28	1.17	1.18	1.17	1.20
10	Biaxis	2.81	2.54	2.95	2.95	2.95	2.95
11	Bilater*	1.17	1.14	1.13	1.13	1.13	1.25
12	Siaxis	2.84	2.67	2.58	2.58	2.58	2.58
13	Silater*	1.32	1.25	1.07	1.07	1.07	1.11
14	Droop	3.14	1.69	−2.38	−2.38	−1.10	−1.10
15	d220*	1244.28	1275.20	1296.94	1296.94	1298.25	1299.82
16	d221*	1330.98	1365.31	1397.00	1397.00	1397.00	1329.46
17	rhs*	1455.78	1475.42	1474.90	1474.90	1474.12	1458.52
18	d122	1793.66	1742.52	1797.22	1797.22	1797.22	1797.22
19	d119	1857.85	1869.09	1839.79	1839.79	1839.79	1839.79
20	d115	1886.69	1879.22	1832.80	1888.26	1832.80	1832.80
21	rmt	1721.27	1729.26	1707.65	1707.70	1707.65	1707.65
22	rmb	1641.14	1668.28	1638.86	1638.86	1639.05	1639.05
23	d124	3402.05	3368.43	3347.04	3347.04	3322.03	3322.03
24	d138	87.83	93.79	87.34	86.09	86.09	86.09
25	d126	−5.10	−1.49	−4.96	−4.93	−4.88	−4.88
26	d90	34.32	41.18	45.39	45.39	45.39	45.39
27	d92	607.66	601.66	645.00	644.22	648.12	648.12
28	d225	25.07	26.55	24.27	24.37	23.24	23.24
29	d226	22.15	27.86	26.10	26.00	25.91	25.91
30	d235	21.17	26.65	22.08	22.85	22.14	22.14
31	d236	27.17	24.88	27.87	27.88	27.87	27.87
32	d230	24.26	23.55	25.55	25.53	25.17	25.17
33	d231	25.72	22.10	27.32	27.32	27.29	27.29
Objective	TPR (CFD)	0.9790	0.9789	0.9877	0.9865	0.9884	0.9863

[a]GA result maximizing TPR with no constraint.
[b]GA result maximizing scarf angle with TPR as a constraint.
[c]Results on the Pareto front of the full-scale model.
[d]Result on the Pareto front of the model with reduced parameter set.

C. Search on Surrogate Models Using Genetic Algorithm

The surrogate model built using the best set of hyperparameters is next searched using a single-objective genetic algorithm (GA) with population size and number of generations set as 60 and 20, respectively. Two individual searches have been carried out using different objective functions. In the first optimization, the total pressure recovery at the fan face is used as an objective function and no constraints are applied. The second search is carried out using the scarf angle as an objective function with a minimum pressure recovery set as a constraint. The search traces from these two optimizations are given in Fig. 5. Results are shown in the columns identified as A and B in Table 3. It is not surprising that when the scarf angle is treated as the objective function and pressure recovery as a constraint, the upper bound for the scarf angle is

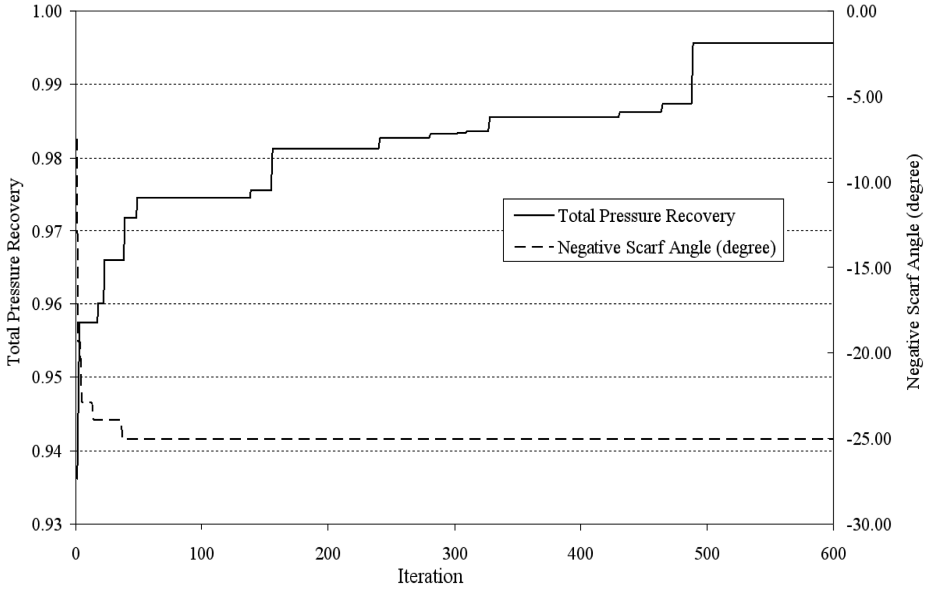

Fig. 5 Convergence histories for total pressure recovery and scarf angle in the single-objective GA search using a surrogate model.

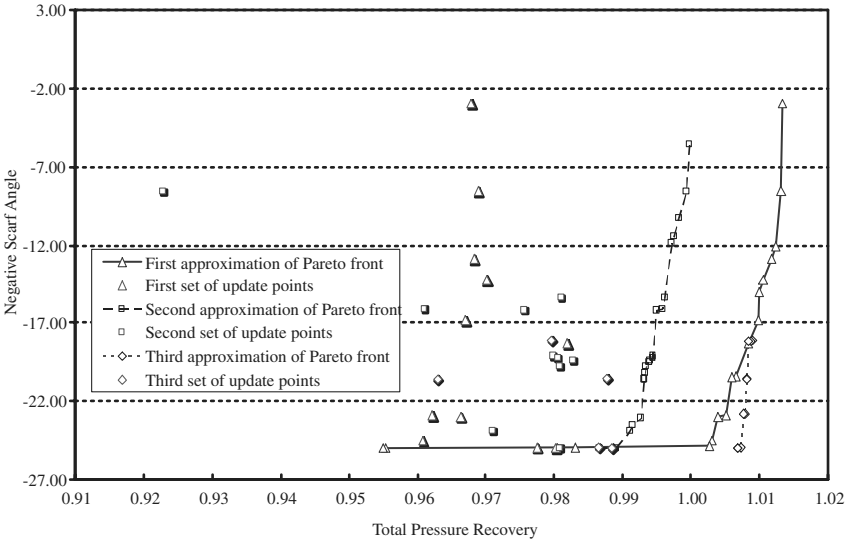

Fig. 6 Update points and approximated Pareto fronts for pressure recovery and scarf angle.

reached while satisfying the pressure recovery ($> = 0.95$). Full CFD models have been used to validate these results obtained from using the surrogate models. However, it is understood that such a high negative scarf angle would become impractical due to constraints in other operating conditions, and, in particular, during takeoff, where the flow would tend to separate for high angles of attack. These results illustrate the diverse, complex relations between total pressure recovery (TPR) and design variables. It shows that a full tradeoff study is necessary to help obtain improved and balanced designs.

D. Search Using Multi-Objective Genetic Algorithm

To obtain a more complete picture regarding the tradeoff relations between the scarf angle and pressure recovery, a multi-objective genetic algorithm is used to obtain the Pareto front for these two quantities. An implementation of NSGA-II [16] is used in the study. An update strategy with the use of surrogate-based Pareto fronts is used to help locate the best points. The update strategy is described as follows:

1) build a kriging model using the best set of hyperparameters from the tuning process;

2) find the Pareto front using the kriging model;

3) for all design points on the Pareto front, if a valid geometry can be produced, obtain the full CFD solution; otherwise, find the nearest valid geometry and obtain the CFD solution for it;

4) add the newly available CFD solutions to the data set and rebuild the kriging model;

5) repeat steps 2 to 4 until the solution converges or computational budget is exhausted.

It should be noted that convergence may not be possible for such a strategy, particularly for high dimensional problems. One of the difficulties in obtaining a converged Pareto front comes from the difficulty in getting an accurate kriging model when the number of variables is large. Another issue in the procedure is that some points on the approximated Pareto front will not lead to valid geometries, and even for valid geometries, problems may arise in the meshing and solution phases to prevent valid solutions being obtained. Nonetheless, this strategy does lead to better designs being produced without resorting to huge numbers of expensive CFD solutions. Three Pareto fronts are shown in Fig. 6, along with update points used. It can be seen that the kriging model overestimates the total pressure recovery at regions close to the Pareto front, which suggests more design points are still required if the kriging model is expected

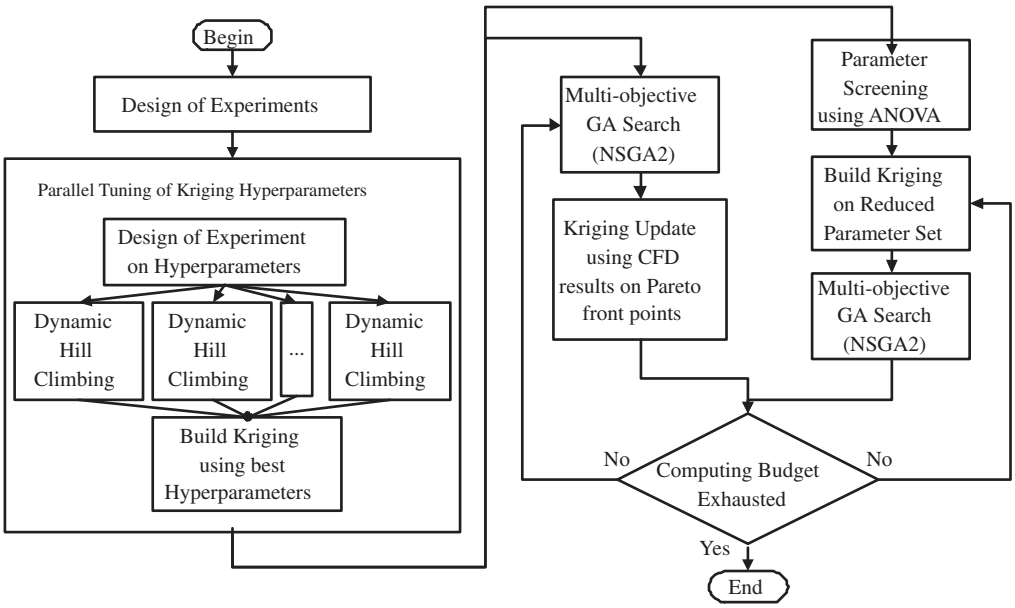

Fig. 7 Flowchart for the complete optimization process.

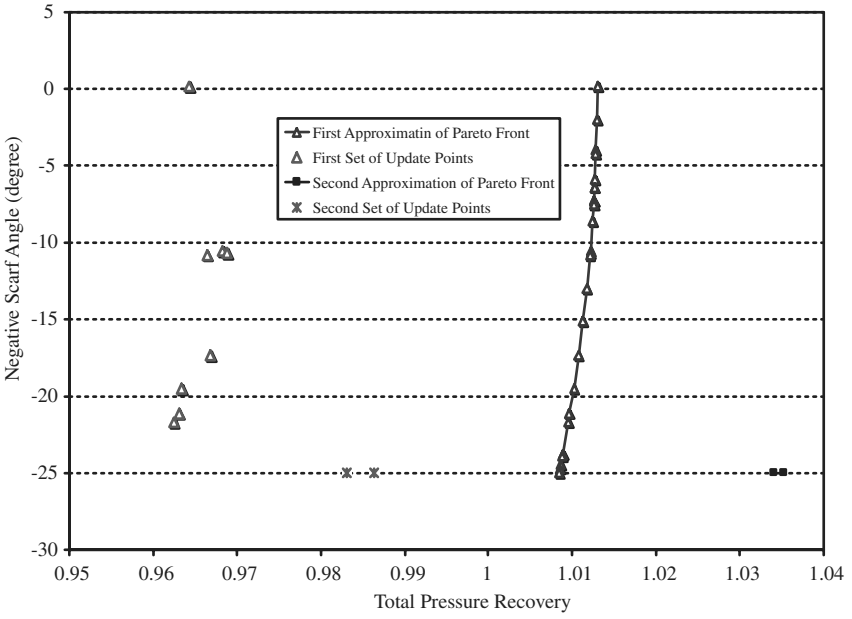

Fig. 8 Update points and approximated Pareto fronts for the reduced-basis problem.

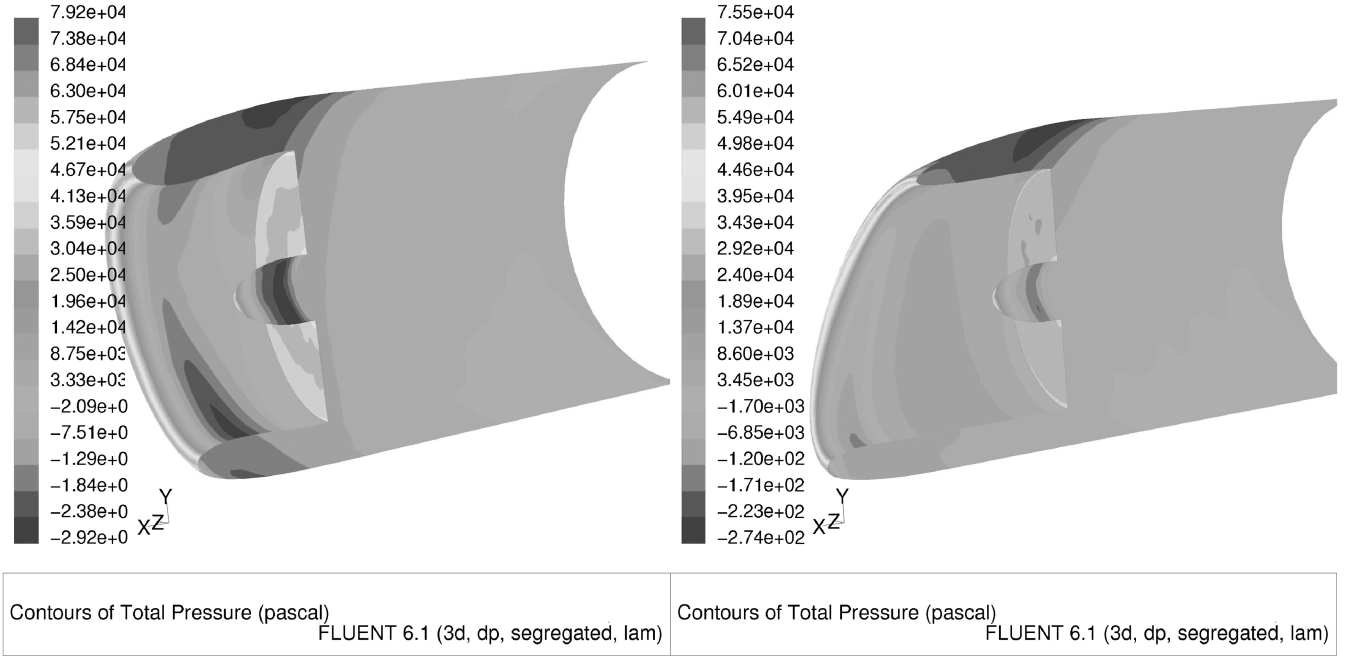

Fig. 9 Comparison between surface pressure distributions on the base and final design.

to achieve an accurate approximation of the Pareto front. On the other hand, some pretty good designs have been found compared to the base design. Three good design points on the Pareto front are summarized in Table 3 (columns C, D, and E) along with the base design and results found using single-objective searches (columns A and B). The complete procedure described above is summarized in Fig. 7.

IV. Reduced-Basis Surrogate Model

Based on the results obtained from Sec. III, a problem with a reduced number of design variables has been formulated and studied. Seven variables are used, which include the six most important variables obtained using the ANOVA techniques set out in previous sections, plus the scarf angle. These variables are identified in Tables 1 and 3 with an asterisk. A series of reduced-basis surrogate models are built by varying these parameters, while leaving the rest of the parameters at values returned by searching the full surrogate models in the previous section (shown in column E of Table 3). A second set of CFD simulations has been carried out using a smaller data set generated on this reduced parameter set. Similar strategies are applied to this problem, and the evolutions of the Pareto fronts are shown in Fig. 8. This reduced-basis model allows the problem to be explored much more efficiently. Compared with results obtained from those using the full parameter set, a design with similar performance has been achieved with significantly less computational expense. The final shape of the nacelle is compared with the base design in Fig. 9, in which the total pressure distributions on the nacelle surfaces are also compared. It can be seen that the pressure gradients on the inlet surfaces and fan face have been improved. However, the result will have to be complemented by further CFD studies on other flow conditions such as crosswind and possible experimental data. Clearly, the full benefit of noise reduction using nacelles with negative scarf angles can only be fully understood with the use of a combined CFD analysis, acoustic analysis, and wind tunnel and flight tests.

V. Summary and Concluding Remarks

This paper presents a preliminary study on the effects of various geometry parameters including negative scarf angle on the subsonic aerodynamic performance of a civil aircraft engine nacelle using response surface modeling, a multi-objective genetic algorithm, and ANOVA techniques. Gaussian process-based surrogate models (kriging) were built using hyperparameter parallel tuning based on results obtained from a CFD flow analysis. Parameter screening techniques were applied to the surrogate models to identify parameters with the most important effects. Multiple Pareto fronts were built using a sequence of kriging models, with CFD results of the best points in previous Pareto fronts being added each time a new kriging model is built.

The approach presented in this paper is generic and provides a useful framework for dealing with optimization problems with large numbers of design variables involving high-fidelity codes. The use of parallel hyperparameter tuning and ANOVA techniques proved to be effective in identifying important variables. Other types of data mining and knowledge-based methods could also be used to improve the efficiency and effectiveness of expensive optimization problems. This is the subject of future work.

Acknowledgments

This research was funded by the U.K. Engineering and Physical Sciences Research Council under Grant GR/R67705/01. The authors are grateful to Ivan I. Voutchkov for the coding of the NSGA-II algorithm in MATLAB.

References

[1] Fisher, M. J., and Self, R. H., "Aeroacoustics Research in Europe: The CEAS-ASC Report on 2001 Highlights," *Journal of Sound and Vibration*, Vol. 258, No. 1, 2002, pp. 1–30.

[2] Jones, M. G., Tracy, M. B., Watson, W. R., and Parrott, T. L., "Effects of Liner Geometry on Acoustic Impedance," AIAA Paper 2002-2446, June 2002.

[3] Abbott, J. M., and Slater, J. W., "Computational Study of the Aerodynamic Performance of Three-Dimensional Subsonic Inlets," AIAA Paper 2001-3886, July 2001.

[4] Nangia, R. K., and Palmer, M. E., "Negatively Scarfed Inlets for Acoustic Reduction, Aerodynamic Performance Assessment," AIAA Paper 2000-0354, Jan. 2000.

[5] Nangia, R. K., and Palmer, M. E., "Inlets with Negative Scarf for Acoustic Reduction, Aerodynamic Assessment at Transonic Speed," AIAA Paper 2000-4409, Aug. 2000.

[6] Reddy, D. R., Reddy, E. S., and Moody, R. E., "Aerodynamic Shape Optimization of a Subsonic Inlet Using Three-Dimensional Euler Computation," *Journal of Propulsion and Power*, Vol. 14, No. 2, 1998, pp. 225–233.

[7] Mason, J. G., Farquhar, B. W., Booker, A. J., and Moody, R. E., "Inlet Design Using a Blend of Experimental and Computational Techniques," *Proceedings of the 18th Congress of ICAS*, AIAA, Washington, D.C., 1992, Vol. 1, pp. 445–454; also International Council of the Aeronautical Sciences Paper ICAS-92-3.3.1.

[8] Smith, A. R., Thorne, R., Gouttenoire, C., Surply, T., and Chanez, P., "Aerodynamic Aspects of Application of Negative Scarf Intake to High Bypass Ratio Civil Turbofans," AIAA Paper 2005-4205, July 2005.

[9] Wilhelm, R., "Inverse Design Methods for Designing Isolated and Wing-Mounted Engine Nacelles," *Journal of Aircraft*, Vol. 39, No. 6, 2002, pp. 989–995.

[10] Lian, Y., and Liou, M.-S., "Multiobjective Optimization Using Coupled Response Surface Model and Evolutionary Algorithm," *AIAA Journal*, Vol. 43, No. 6, 2005, pp. 1316–1325.

[11] Jin, Y., "A Comprehensive Survey of Fitness Approximation in Evolutionary Computation," *Soft Computing Journal*, Vol. 9, No. 1, 2004, pp. 3–12.

[12] Kim, T. S., and Kim, Y. Y., "Multiobjective Topology Optimization of a Beam Under Torsion and Distortion," *AIAA Journal*, Vol. 40, No. 2, 2002, pp. 376–381.

[13] Epstein, B., and Peigin, S., "Robust Hybrid Approach to Multiobjective Constrained Optimization in Aerodynamics," *AIAA Journal*, Vol. 42, No. 8, 2004, pp. 1572–1581.

[14] Corne, D. W., Jerram, N. R., Knowles, J. D., and Oates, M. J., "PESA-II: Region-Based Selection in Evolutionary Multiobjective Optimization," *Proceedings of the Genetic and Evolutionary Computation Conference*, Morgan Kaufmann, Scan Francisco, CA, 2001, pp. 283–290.

[15] Knowles, J. D., and Corne, D. W., "The Pareto Archived Evolution Strategy: A New Baseline Algorithm for Multiobjective Optimization," *1999 Congress on Evolutionary Computation*, IEEE, Piscataway, NJ, 1999, pp. 98–105.

[16] Deb, K., Pratap, A., Agarwal, S., and Meyarivan, T., "A Fast and Elitist Multi-Objective Genetic Algorithm: NSGA-II," *IEEE Transaction on Evolutionary Computation*, Vol. 6, No. 2, 2002, pp. 181–197.

[17] Horn, J., Hafpliotis, N., and Goldberg, D. E., "A Niched Pareto Genetic Algorithm for Multiobjective Optimization," *Proceedings of the First IEEE Conference on Evolutionary Computation*, IEEE World Congress on Computational Intelligence, IEEE, Piscataway, NJ, 1994, pp. 82–87.

[18] Knowles, J. D., and Corne, D., "M-PAES: A Memetic Algorithm for Multiobjective Optimization," *Proceedings of the 2000 Congress on Evolutionary Computation*, IEEE, Washington, D.C., 2000, pp. 325–332.

[19] Knowles, J. D., and Corne, D., "Memetic Algorithms for Multiobjetive Optimization: Issues, Methods, and Prospects," *Recent Advances in Memeti Algorithms*, Vol. 166, Springer, Berlin, 2004, pp. 313–352.

[20] Samareh, J. A., "Survey of Shape Parameterization Techniques for High-Fidelity Multidisciplinary Shape Optimization," *AIAA Journal*, Vol. 39, No. 5, 2001, pp. 877–884.

[21] Langer, H., Puhlhofer, T., and Baier, H., "An Approach for Shape and Topology Optimization Integrating CAD Parameterization and Evolutionary Algorithms," AIAA Paper 2002-5498, Sept. 2002.

[22] Song, W., Keane, A. J., Rees, J., Bhaskar, A., and Bagnall, S., "Turbine Blade Bir-Tree Root Design Optimization Using Intelligent CAD and Finite Element Analysis," *Computers and Structures*, Vol. 80, No. 24, 2002, pp. 1853–1867.

[23] Haimes, R., and Merchant, A., "The Synergistic Use of CAD for Tightly Coupled Analysis and Design," AIAA Paper 2005-4986, June 2005.

[24] Song, W., Keane, A. J., and Cox, S. J., "CFD-Based Shape Optimization with Grid-Enabled Design Search Toolkits," *Proceedings of the UK e-Science All Hands Meeting*, UK National e-Science Centre, Edinburgh, U.K., Sept. 2003, pp. 619–627.

[25] Santner, T. J., Williams, B. J., and Notz, W. I., *The Design and Analysis of Computer Experiments*, Springer–Verlag, New York, 2003.

[26] Mckay, M. D., Bechman, R. J., and Conover, W. J., "A Comparison of Three Methods for Selecting Values of Input Variables in the Analysis of Output from a Computer Code," *Technometrics*, Vol. 21, No. 2, 1979, pp. 239–245.

[27] Booker, A. J., Frank, P. D., Dennis, J. E., Moore, D. W., and Serafini, D. B., "Managing Surrogate Objectives to Optimize a Helicopter Roter Design—Further Experiments," AIAA Paper 98-4717, 1998.

[28] Booker, A. J., Dennis, J. E., Frank, P. D., Serafini, D. B., and Torczon, V., "Optimization Using Surrogate Objectives on a Helicopter Test Example," Rice University, Center for Research on Parallel Computation CRPC-TR97734-S, Dec. 1997; also Boeing Rept. SSGTECH-97-027, Rice CAAM TR97-31.

[29] Welch, W. J., Buck, R. J., Sack, J., Wynn, H. P., Mitchell, T. J., and Morris, M. D., "Screening Predicting and Computer Experiments," *Technometrics*, Vol. 34, No. 1, 1992, pp. 15–25.

[30] Chang, P. B., Williams, B. J., Bhalla, K. S. B., Belknap, T. W., Santner, T. J., Notz, W. I., and Bartel, D. L., "Design and Analysis of Robust Total Joint Replacements: Finite Element Model Experiments with Experimental Variables," *Journal of Biomechanical Enigneering, Transactions of the ASME*, Vol. 123, No. 3, 2001, pp. 239–246.

[31] Craig, K. J., Stander, N., Dooge, D. A., and Varadappa, S., "Automotive Crashworthiness Design Using Response Surface-Based Variable Screening and Optimization," *Engineering Computations*, Vol. 22, No. 1, 2005, pp. 38–61.

[32] Montgomery, D. C., *Design and Analysis of Experiments*, 5th ed., Wiley, New York, 2000.

J. Samareh
Associate Editor